Journal of Industrial and Engineering Chemistry 69 (2019) 315–323

Contents lists available at ScienceDirect

Journal of Industrial and Engineering Chemistry

journal homepage: www.elsevier.com/locate/jiec

Fabrication and characterization of graphene oxide–titanium dioxide nanocomposite for degradation of some toxic insecticides

Nagi M. El-Shafai[a,b], Mohamed E. El-Khouly[c,d,*], Maged El-Kemary[b,c,*], Mohamed S. Ramadan[a], Aly S. Derbalah[e], Mamdouh S. Masoud[a,*]

[a] Department of Chemistry, Faculty of Science, Alexandria University, Alexandria, Egypt
[b] Institute of Nanoscience and Nanotechnology, Kafrelsheikh University, Kafr El-Sheikh 33516, Egypt
[c] Department of Chemistry, Faculty of Science, Kafrelsheikh University, Kafr El-Sheikh 33516, Egypt
[d] Institute of Basic and Applied Sciences, Egypt-Japan Institute of Basic and Applied Sciences (E-JUST), Alexandria, Egypt
[e] Pesticides Chemistry and Toxicology Department, Faculty of Agriculture, Kafrelsheikh University, Kafr El-Sheikh 33516, Egypt

ARTICLE INFO

Article history:
Received 19 May 2018
Received in revised form 5 June 2018
Accepted 26 September 2018
Available online 4 October 2018

Keywords:
Graphene oxide
Titanium dioxide
Nanocomposite
Photodegradation
Insecticides

ABSTRACT

Graphene oxide–titanium dioxide (GO@TiO_2) nanocomposite with mean diameter size of 14 nm has been fabricated, characterized, and used as photocatalyst for degradation of two highly toxic insecticides, namely carbaryl and imidacloprid. Characterizations of GO@TiO_2 have been carried out using various analytical and spectroscopic techniques. Compared to TiO_2NPs, the fabricated GO@TiO_2 nanocomposite has advantage of its smaller band gap. The finding that the photocatalytic degradation of the examined insecticides by the fabricated GO@TiO_2 is more efficient compared to that of TiO_2NPs suggests the superiority for using the fabricated GO@TiO_2 nanocomposite for degradation of the examined toxic insecticides.

Introduction

Water is the most important source of life as it required for all human activities. Due to the rapid developments of economics and industries, water pollution is one of the biggest problems in the world. Among the most serious pollution sources in the developing countries, pesticides cause serious health and environmental problems [1]. Carbamate insecticides such as carbaryl are highly toxic and widely used as insecticides, acaricides, nematocides, herbicides, and molluscicides for protection of crops. Widespread use of carbamates in agriculture increases their residues in soil and water [2]. In addition, imidacloprid is one of the commonly insecticides in agriculture that have been demonstrated harmful effects [3]. According to US EPA reports, imidacloprid is high toxic for the aquatic invertebrates [4].

Several approach have been reported for pesticides removal from the aquatic environment, e.g., adsorption, membrane separation, fluid extraction, etc [5,6]. Among these methods, photocatalytic degradation by the newly fabricated semiconducting nanoparticles is an effective technology in the environmental application [7–9], in particular for converting the pesticides into friendly compounds [10–13]. In particular, TiO_2 semiconductor was extensively examined as photocatalyst for its advantages of wide energy gap, chemical and thermal stability, low cost, unique optical and electronic properties, ease of fabrication, and wide compatibility [14]. These properties render TiO_2 as efficient photocatalyst for decomposition of various pollutants in an aqueous media. On the other hand, TiO_2 suffers from its high band gap (only in the UV region, 3.2 eV), high charge carrier recombination, and low surface area. These undesired properties restrict its uses in various applications. For overcoming these limitations of using TiO_2 and to extend its light absorption in the visible range, the combination of TiO_2 with various carbon nanostructures (carbon nanotube, graphene, etc) attracted much attention in the recent years. Compared with other carbon materials, graphene with its two dimensional structure attracted much attention for its excellent mobility of charge carriers, large specific surface area, flexible structure, unique optical and electronic properties [8,14,15].

Based on their unique properties, the combination between GO and semiconductor TiO_2 forming GO@TiO_2 nanocomposite that would enhance the photocatalytic performance [16–21]. In such GO@TiO_2 nanocomposite, GO can work as an acceptor/transporter of the photogenerated electrons for TiO_2 nanoparticles (NPs) and reduced the recombination of photogenerated electron–holes of

* Corresponding author.
E-mail address: mohamed.elkhouly@ejust.edu.eg (M.E. El-Khouly).

https://doi.org/10.1016/j.jiec.2018.09.045
1226-086X/

TiO_2. Keeping it into consideration, we report herein the photocatalytic efficiency of two pesticides, namely carbaryl and imidaclporid by using titanium dioxide (TiO_2) and graphene oxide–titanium dioxide nanocomposite ($GO@TiO_2$) (Fig. 1). According to our information's, such studies for photodegradation of these two toxic pesticides by the modified graphene with TiO_2 are rare in the literature. The fabricated $GO@TiO_2$ nanocomposite has been well characterized by using X-ray diffraction (XRD), transmission electron microscopy (TEM), scanning electron microscopy (SEM), zeta potential, and Fourier transform infrared spectroscopy (FTIR) techniques. The photocatalytic degradation of carbaryl and imidaclporid by the fabricated $GO@TiO_2$ has been studied by using steady-state absorption and fluorescence techniques.

Experimental section

Materials and instruments

The two examined insecticides namely, 1-naphthyl methylcarbamate(Carbaryl), and *N*-{1-[(6-Chloro-3-pyridyl)methyl]-4,5-Dihydro-imidazol-2-yl}nitramide (Imidacloprid) were purchased from Sigma-Aldrich Company Ltd. The Old Brickyard, New Road Gillingham Dorset SP8 4 XT United kingdom. Titanium (IV) *n*-isobutoxide was obtained from Strem chemical. Graphite, potassium hydroxide and ethanol were purchased from Sigma-Aldrich. All used chemicals in this study were reagent grade and used without any further purification.

UV–vis absorption spectra were measured using a Shimadzu UV-2450 spectrophotometer model. Fluorescence measurements were carried out by using Shimadzu RF-5301PC spectrofluorometer. Fourier transform infrared (FT-IR) spectra were measured using a JASCO spectrometer 4100 using the KBr pellet technique. The X-ray diffraction (XRD) measurements were conducted by using a Shimadzu 6000–XRD, X-ray diffractometer using Cu Kα radiation ($\lambda^1/_4$1.54056 Å). Transmission electron microscopy (TEM) images were recorded by a JEOL 2010 microscope operating at an accelerating voltage of 200 kV. While the morphology of the surface was estimated using scanning electron microscopy (SEM), JEOL(JSMIT100) 30 kV. Zeta potential data were obtained by Brookhaven zeta potential/particle size analyzer. The specific surface area, pore volume and the pore structure were determined by N_2 adsorption technique using Nova touch LX^3 analyzer.

Photocatalytic degradation of the examined insecticides

The efficiency of TiO_2 nanoparticles and $GO@TiO_2$ nanocomposite were determined for photodegradation of some insecticides under UV light source at 365 nm. The concentration of examined insecticides was 100 ppm, 5 mg of TiO_2 nanoparticles and GO–TiO_2 nanocomposite were dispersed in 10 ml water. The photocatalytic measurements were performed with different times after exposed to UV light at wavelength of 365 nm. $OH^{\bullet}$ radicals were generated during the reaction, which can be decompose the pesticides. Photodegradation of the examined insecticides was detected by using steady-state absorbance and fluorescence techniques. The adsorption activity of GO for insecticides, such as, carbaryl, and imidaclporid was evaluated. Furthermore, the activities property of TiO_2 nanoparticles and $GO@TiO_2$ nanocomposite in the absence of light were examined.

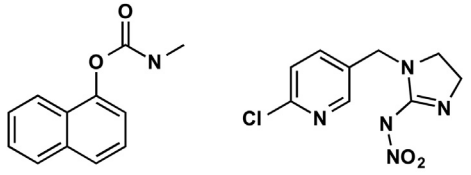

Carbaryl Imidacloprid

Fig. 1. Chemical structure of the examined insecticides.

Synthesis of nanocomposite

Synthesis of graphene oxide nanostructure

Water dispersions and solid of graphite oxide were prepared from natural graphite powder using a modified Hummers and Offeman's method [22,23]. In a typical reaction, to a glass beaker 8 g of graphite flakes (Sigma Aldrich), 8 g of NH_4NO_3 and 368 ml of 98% (w/w) H_2SO_4 were added, and mixed under stirring in an ice bath for 1 h. Then, 40 g of $KMnO_4$ was slowly added to the mixture in an ice bath, and thoroughly mixed for 1 h, the solution color becomes green. After that, the beaker placed in a 35 °C water bath, and the solution was stirred for about 1 h to form a thick paste. Then 640 ml of high-purity water was added to the formed paste, and stirred at 90 °C for 1 h, which change the solution color to be brown. Finally, 1600 ml of water was added, followed by the slow addition of 48 ml of H_2O_2 (30%), meanwhile the color of the solution turned from dark brown to yellow. The solid filtered, washed with 10% HCl aqueous solution (3.2 l) to remove metal ions and washed with high-purity water several times until pH became 6. The resulting GO was dried at 45 °C for 24 h. The crystalline structure of dried powder was identified by XRD (Shimadzu 6000 model) using Cu Kα (λ = 1.5418 Å) as incident radiation. Refinement was carried out from a starting model based on information given in the Inorganic Crystal Structure Database (ICSD). The morphology of the GO synthesized was evaluated by transmission electron microscopy (TEM, JEOL 2100) under maximum acceleration voltage of 200 kV.

Synthesis of titanium dioxide

A 6 ml of titanium (IV) *n*-isobutoxide 98% was added dropwise to mixture of ethanol–water (4:1) at 90 °C. The resultant has been reflux for 2 h at 90 °C, the color of mixture was changed into white precipitate (ppt). The obtained precipitate was centrifuged at 6000 rpm, then washed with deionized (DI) water and ethanol for several times, then dried at 50 °C, and calcined at 470 °C for 2 h [24].

Synthesis of $GO@TiO_2$ nanocomposite

The fabrication process was carried out by dispersing 1 gm of TiO_2 nanoparticles that prepared in a previous step in 50 ml water for 30 min by ultrasonic and a drop wise has been added to 0.04 g of GO nanosheet which dispersed in 100 ml water. After that, the mixture was mixed by ultrasonic for 3 h and the obtained precipitate was centrifuged at 6000 rpm. Then washed with DI water for several times and dried at 50 °C [25].

Results and discussion

Characterization of $GO@TiO_2$ nanocomposite

XRD analysis

Fig. 2 showed the XRD pattern of the pure graphite powder, synthesized GO, TiO_2 NPs, and $GO@TiO_2$ nanocomposite powder. The XRD analysis exhibits the (001) diffraction peak of GO (10.9°) [26,27], which is larger than that of the pure graphite (26°). This can be rationalized by the presence of the oxygenated functional groups on carbon sheets of GO [17,28]. The XRD pattern of TiO_2 NPs showed typical diffraction peak of anatase phase (25.16°, 37.78°, 47.89°, 53.85°, 54.83°, 62.64° and 74.88°) [29], without any

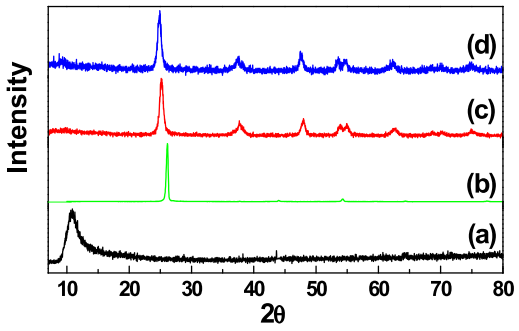

Fig. 2. XRD patterns of: (a) graphene oxide, (b) graphite, (c) TiO_2 NPs, and (d) GO–TiO_2 nanocomposite.

contribution of rutile or brookite phases. Compared with other phases, the anatase phase exhibited high surface area and its slower charge carrier recombination compared with other phases. When turning to GO@TiO_2 nanocomposite, the XRD pattern showed values the diffraction peaks at 24.84°, 37.42°, 47.59°, 54.80°, 62.31° and 74.69° [30]. The absence of typical peak of GO may due to the disruption and well exfoliation of GO in the nanocomposite and/or the loading of metal oxide into the surface of GO oxide.

The main crystallite size of GO and metal oxide nanocomposite was calculated based on the Debye-Scherrer's formula (Eq. (1)):

$$D = K\lambda/\beta\cos\theta \quad (1)$$

where, K is a constant representing shape factor (~0.9), λ is the wavelength of the X-ray source (1.5405 Å), β is the full width at half maximum of the diffraction peak and θ is the angular position of the peak. The average crystallite sizes were determined to be 15 nm and 14–24 nm for TiO_2 and GO@TiO_2, respectively. This finding suggests that the anchoring of GO with TiO_2 NPs nanocomposite has little influence on the crystallite size of phase structure of TiO_2 NPs.

HR-TEM analysis

The morphologies of GO, TiO_2 NPs and GO@TiO_2 nanocomposite were characterized by high resolution TEM images with different magnifications to illustrate the shape of the particles. As shown in Fig. 3, GO showed a good nanosheet form, while TiO_2 NPs showed good dispersion nano-spherical shape. However, GO@TiO_2 nanocomposite showed like nano-spherical shape loading into the GO sheet with an average size of about 15–24 nm, which is in a good agreement with that observed by the XRD measurements.

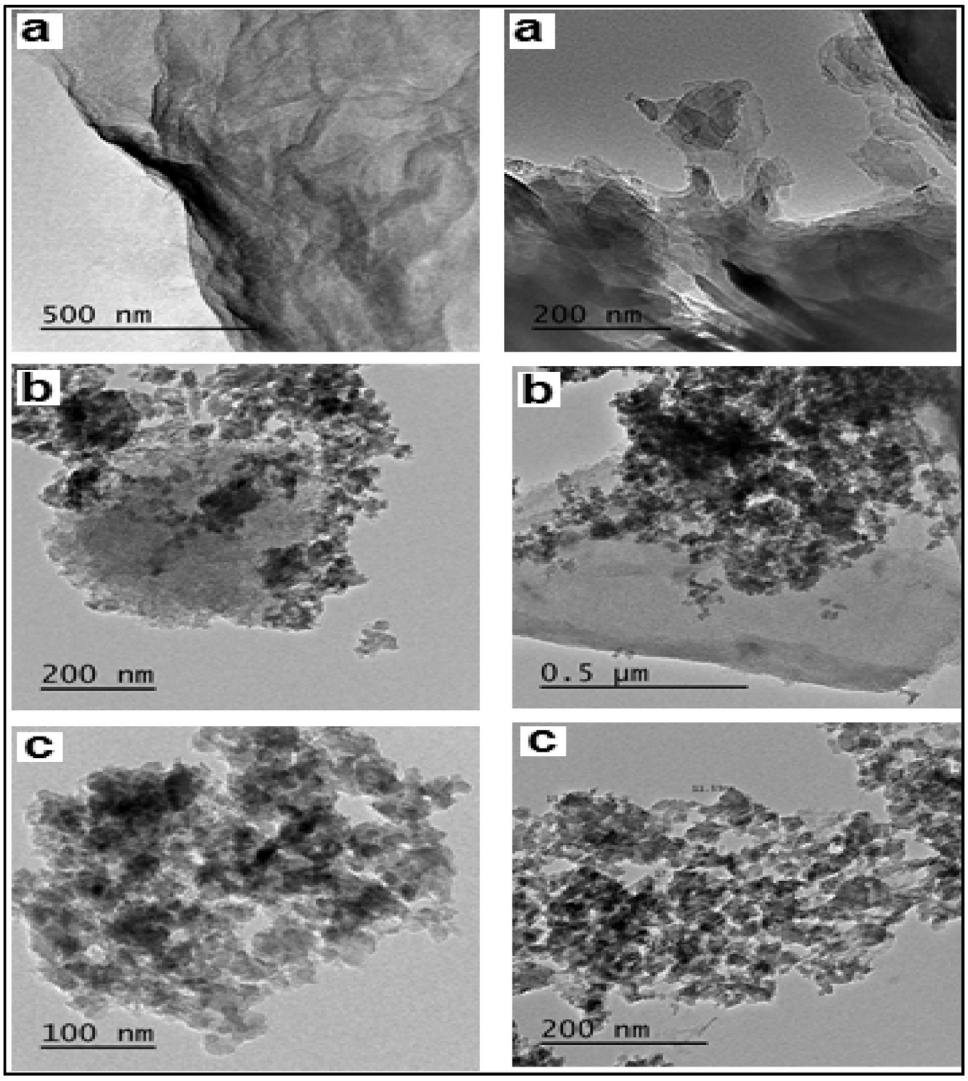

Fig. 3. HR-TEM image of: (a) GO, (b) GO@TiO_2 nanocomposite, and (c) TiO_2 NPs.

SEM analysis

The fabricated GO@TiO_2 nanocomposite was characterized by scanning electron microscopy (SEM) technique with different magnifications to exhibit its spherical morphology. As shown in Fig. 4, the surface of GO nanosheet was packed densely by TiO_2 NPs with average sizes from 15 to 17 nm indicating a good combination between graphene oxide and TiO_2. GO nanosheets seem to act as bridges that connect with different TiO_2 NPs and increase the separation of the photogenerated electron-hole pairs. This confirms the distribution of TiO_2 nanoparticles on the surface of GO sheets with slightly agglomeration of metal oxide nanoparticles. The samples were analyzed using EDX with uniform particle morphology (Supporting information, Fig. S1).

UV-spectroscopy analysis

The absorption spectrum of GO exhibited an absorption peak with maximum at ~228, which is due to $\pi \rightarrow \pi^*$ transitions of the aromatic C=C bonds [12,26,31], while the absorption maximum of GO–TiO_2 was clearly observed at 260 nm (Supporting information, Fig. S2). Compared with TiO_2NPs, the absorption band of GO@TiO_2 nanocomposite shifted to the visible light region that rationalized by the hybridization of C2p and O2p atomic orbits to create a new valence band.

The band gap values of the fabricated GO@TiO_2, as well as the control of GO and TiO_2 were calculated from Tauc (Eq. (2)) [32,33].

$$\alpha h\upsilon = A(h\upsilon - E_g)^n \quad (2)$$

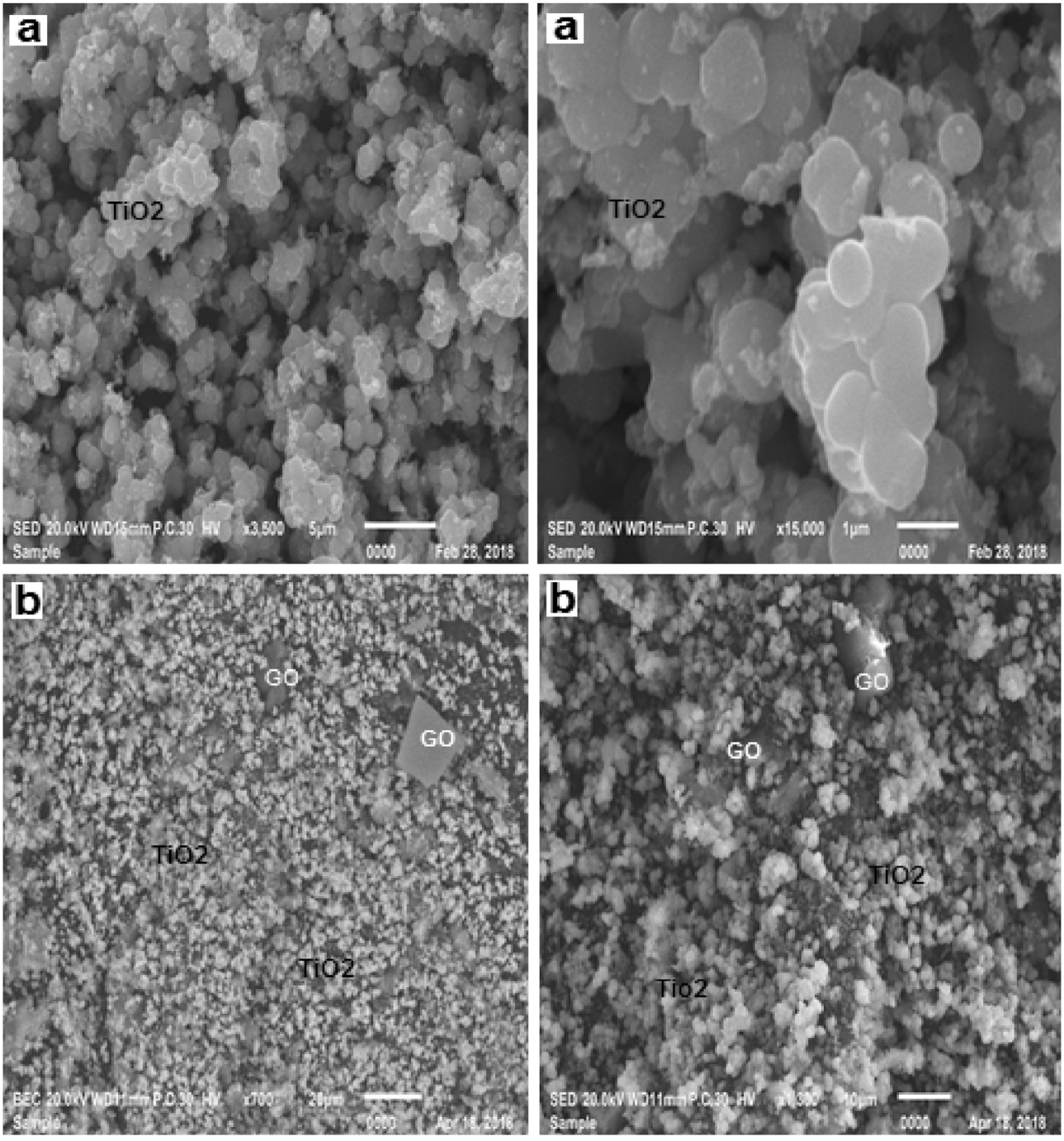

Fig. 4. SEM images of: (a) TiO_2 NPs and (b) GO@TiO_2 nanocomposite.

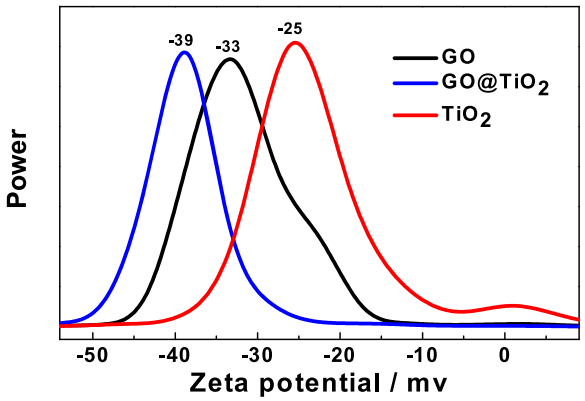

Fig. 5. Zeta potential of GO, TiO_2 and GO@TiO_2 in water.

where α is absorption coefficient, υ is the frequency of light, h is Planck's constant, $h\upsilon$ is the photon energy, A is a proportionality constant, E_g is the band gap and n = 1/2 for the direct transitions [34]. The band gap values were found to be 4.00, 3.50, and 3.78 eV for GO, GO@TiO_2 and TiO_2, respectively.

Zeta potential analysis

Zeta potential technique has been used for detection the stability of the fabricated GO@TiO_2 nanocomposite in the solution and understanding the charge of the surface. As shown in Fig. 5, the results show that particles are negatively charged for GO (−33), TiO_2 (−25) and GO@TiO_2 (−39), revealing high stability of colloidal dispersions of particles in water. Based on these values, one can say that the fabricated GO@TiO_2 nanocomposite exhibited higher dispersion than TiO_2NPs.

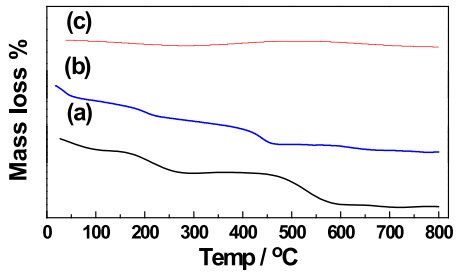

Fig. 6. TGA diagrams of: (a) GO, (b) GO@TiO_2 nanocomposite and (c) TiO_2NPs.

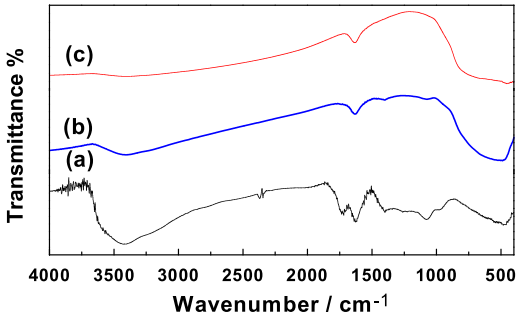

Fig. 7. FT-IR spectra of: (a) GO (a), (b) GO@TiO_2, and (c) TiO_2.

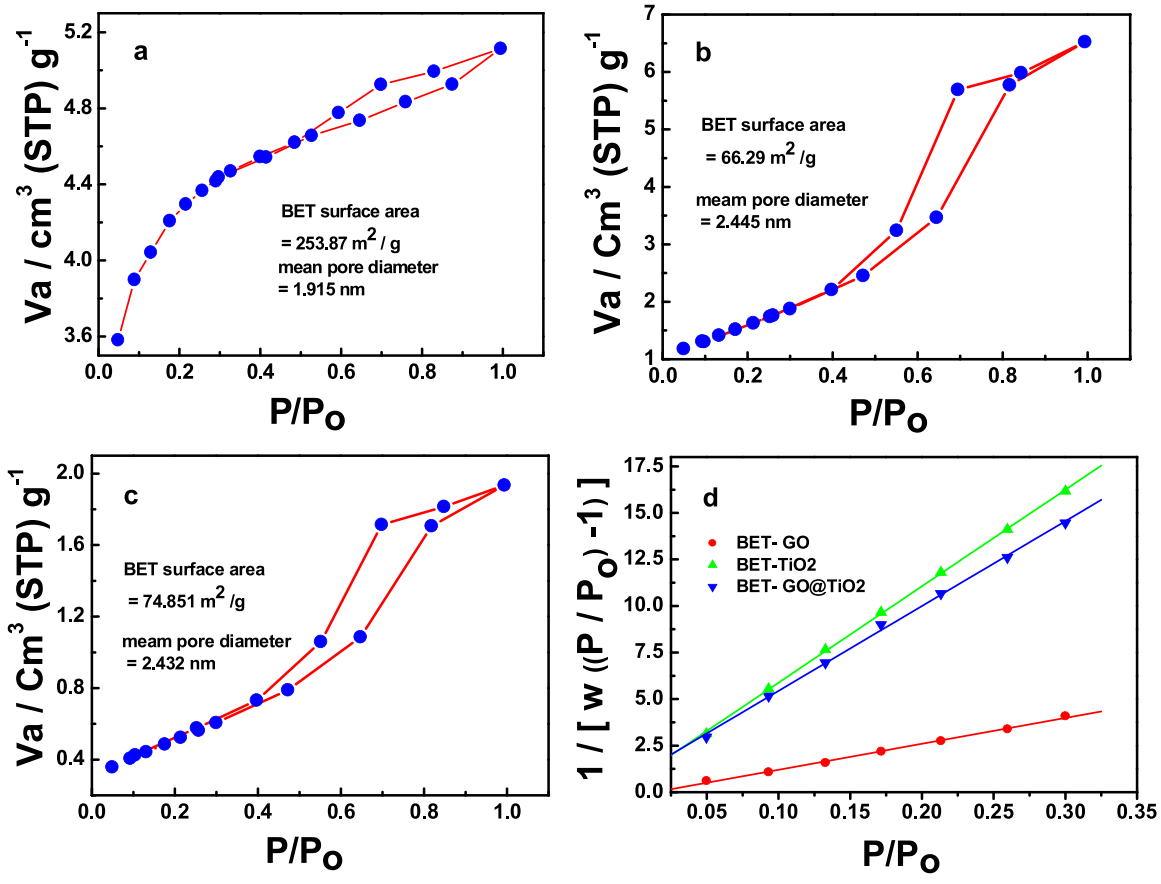

Fig. 8. BET N_2 adsorption/desorption isotherm curve of: (a) GO, (b) TiO_2, and (c) GO@TiO_2. (d) Langmuir fits from the N_2 adsorption data for GO nanosheet, TiO_2 nanorod and GO@TiO_2 nanocomposite.

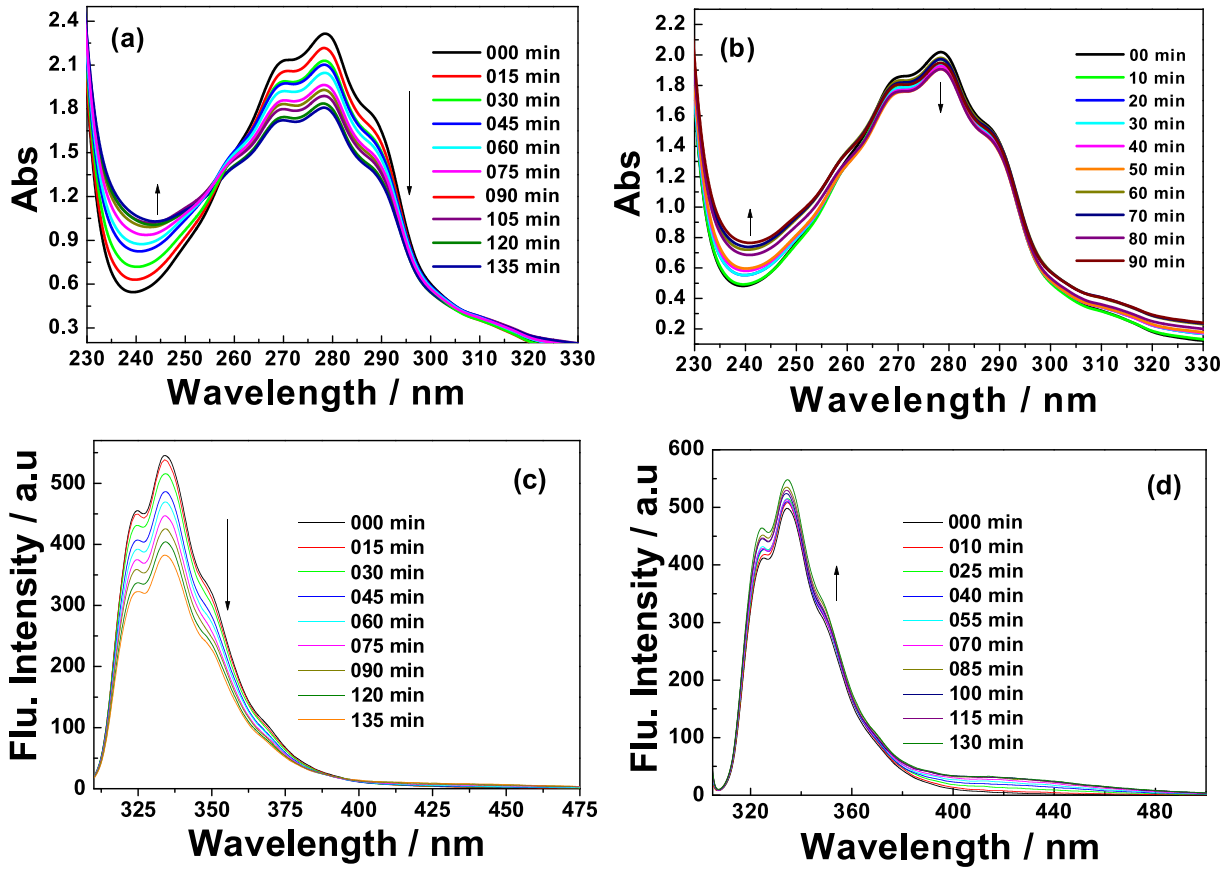

Fig. 9. UV–vis absorption spectra of carbaryl (50 μl from 100 ppm) in the presence of: (a) GO@TiO_2 (0.1 ml from 0.005 g/10 ml), and (b) and TiO_2 (0.1 ml from 0.005 g/10 ml) under UV-light in water at the indicated time intervals. Fluorescence spectra of carbaryl (50 μl from100 ppm) in the presence of: (c) GO@TiO_2 (0.1 ml from 0.005 g/10 ml), and (d) TiO_2 NPs upon using 300 nm excitation light at the indicated time intervals.

Thermal analysis

Fig. 6 shows the thermogravimetric analysis (TGA) diagrams of GO, TiO_2 and GO@TiO_2 at temperatures in the range of 25–700 °C. Thermal analysis curve of TiO_2NPs is straightly line, the total decomposition elements and residue percentages are 0.972 and 99.028%, respectively, this stability in results mean that TiO_2 has been completely formed as a pure metal oxide. The thermogram curve of GO displays a weight loss of up to 200 °C due to the removal of humidity and decomposition of oxygen functional group and release of CO_2 gas [17]. The skeleton of GO is decomposed through four successive steps (first step from 25 to 100 °C, second step from 150 to 280 °C, third step from 450 to 590 °C, and the fourth step from 650 to 710 °C). When turning to GO@TiO_2 nanocomposite, the thermogram curve was accompanied with the decomposition of graphene oxide steps, this emphasis the formation of TiO_2 on the surface of GO. The finding that GO@TiO_2 nanocomposite showed higher thermal stability than GO nanoparticles may be due to the strong interaction exists between GO and TiO_2 NPs in the fabricated nanocomposite.

FT-IR analysis

Fig. 7 shows the FT-IR spectra of the fabricated GO@TiO_2 nanocomposite, as well as GO, and TiO_2 NPs. GO showed peaks at 3400 and 1620 cm^{-1} due to the stretching vibration of (OH) group and the skeletal vibration of GO sheets, respectively. However, the strong peaks at 1730, 1370, 1220, 1165 and 1058 cm^{-1} assigned to stretching vibration of oxygen containing functional groups carboxyl (C=O), carboxyl (C—O), epoxy (C—O), carboxyl (C—OH) and alkoxy (C—O), respectively [35–37]. This indicates numerous oxygen containing functional groups on the GO surface. Anatase phase of TiO_2 exhibits low frequency bands in 500–850 cm^{-1} due to the Ti—O bending vibration and stretching modes. In addition, a broad peak observed in between 3500 to 3000 cm^{-1} can be assigned to stretching vibration of the surface hydroxyl (—OH) groups on the surface TiO_2 nanoparticles [38].

Brunauer–Emmett–Teller theory (BET) studies

Nitrogen adsorption-desorption full isotherm has been used for detecting the surface properties for GO, TiO_2 and GO@TiO_2. The loop of isotherm shown in Fig. 8 was of type (IV) with a H1 hysteresis loop ($0.4 < P/Po > 0.95$), this mean that the surface includes a high degree of pore size uniformity. The result showed that surface has one type of pores, mesopores (diameter 2–50 nm) [39,40]. BET surface area (SBET), for GO, TiO_2 and GO@TiO_2, were determined to be 253.87, 66.29 and 74.8513 m^2/g, respectively. Total pore volume (VP) and mean pore diameter (rp) were 1.915, 2.445 and 2.432 nm for GO, TiO_2 and GO@TiO_2, respectively (Supporting information, Fig. S3).

Photocatalytic degradation studies

Photocatalytic degradation of insecticides under UV irradiation

Photocatalytic degradation processes of the examined insecticides (carbaryl and imidaclporid) using GO nano sheet, TiO_2 NPs and GO@TiO_2 nanocomposite under UV irradiation (at 365) nm was examined by using steady-state absorption and fluorescence techniques. As seen from Fig. 9, the maximum absorption band of carbaryl was recorded at 278 nm. Upon irradiation by using 365 nm, the absorption band of carbaryl decreased in the presence of GO@TiO_2 at the indicated time intervals (Fig. 9a). In contrast, the

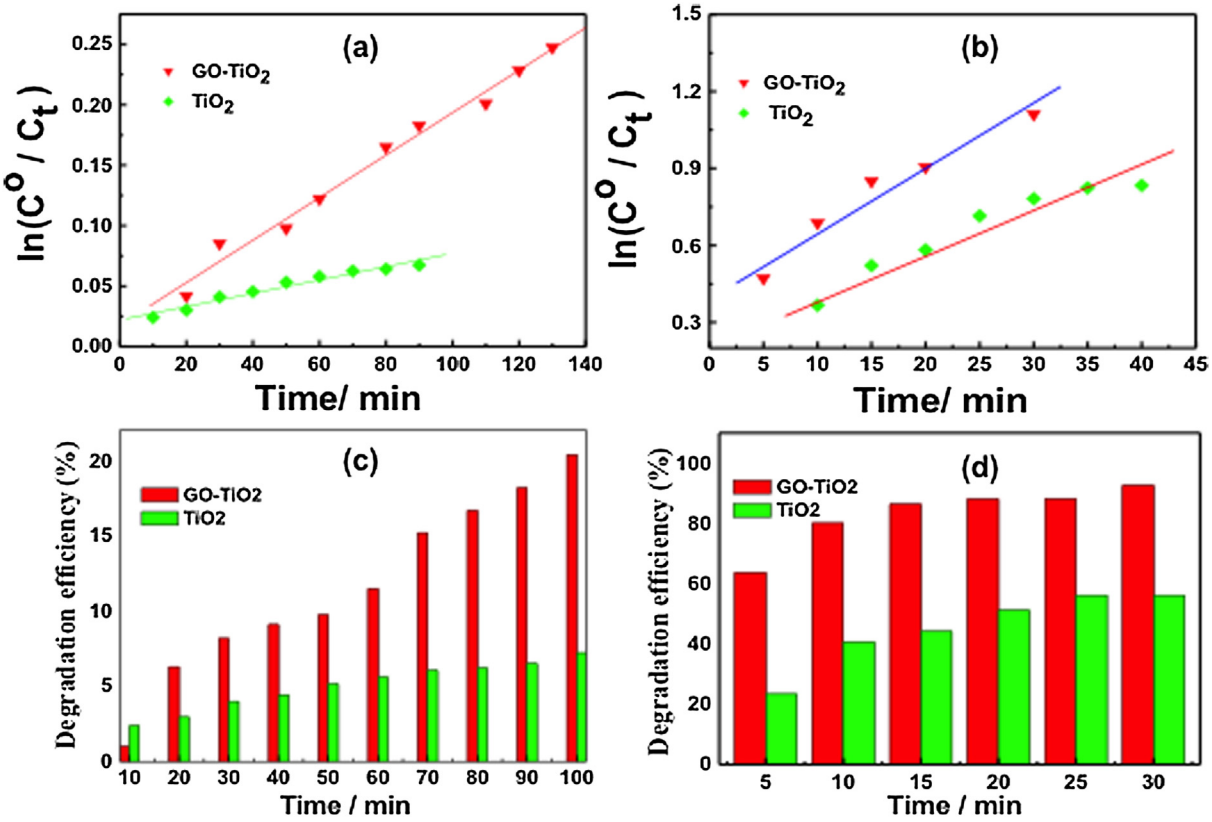

Fig. 10. (Upper figures) Linear plot of ln (C_o/C_t) with irradiation time in water for degradation of: (a) carbaryl and (b) imidacloprid with GO@TiO_2 and TiO_2 (□ = 365 nm). (Lower figures) Photodegradation efficiency (%) of: (c) carbaryl and (d) imidacloprid with GO@TiO_2 and TiO_2 at different times of irradiation; $□_{ex}$ = 365 nm.

absorption spectra of carbaryl showed only small decrease in the presence of TiO_2 NPs (Fig. 9b). This finding indicates that the degradation process of carbaryl pesticide takes place more efficient in the presence of GO@TiO_2 nanocompostie compared to that of TiO_2.

The steady-state fluorescence measurements showed the same track of the absorption measurements. As seen, the fluorescence emission band of carbaryl was observed at around 340 nm. As seen from Fig. 9(c,d), the fluorescence band showed significant quenching in the presence of GO@TiO_2 nanocompostie, but not TiO_2 NPs. This observation is in a good agreement with the steady-state absorption measurements. Similar absorption and fluorescence features were observed upon treating imidacloprid with GO@TiO_2 nanocompostie and TiO_2NPs (Supporting information, Fig. S4).

The rate constants of first order reaction were determined from Eq. (3):

$$\ln(C/C_o) = -k_{obs}\,t \quad (3)$$

where C^o (mg/l) is the initial dye concentration, and k_{obs} depends on the initial concentration (C^o) [41]. The degradation rates (k) of carbaryl in the presence of TiO_2 NPs and GO@TiO_2 nanocomposite were calculated to be 0.00176 and 0.05982 min^{-1} for carbaryl, respectively (Fig. 10a). Similar trend was observed for treating of imidacloprid with TiO_2 NPs ($k = 0.000551\ min^{-1}$) and GO@TiO_2 nanocomposite ($k = 0.0227\ min^{-1}$) (Fig. 10b).

The efficiency of the photocatalytic degradation process was determined from Eq. (4) [42]:

$$E(\%) = ([A_o - A_t]/A_o) \times 100 \quad (4)$$

where A_o and A_t are the absorbance changes of insecticides with the time under light irradiation, respectively [43]. The efficiency of photocatalytic process of carbaryl was found to be 22% and 7% in the presence of GO@TiO_2 and TiO_2, respectively (Fig. 10c). In a similar trend, Fig. 10d illustrates that 92.6% and 56.6% of imidacloprid has been decomposed in the presence of GO@TiO_2 and TiO_2, respectively. This finding showed clearly the significant effect of GO@TiO_2 in increasing the rates and efficiencies of the degradation process compared to the TiO_2 NPs. The higher photo-degradation efficiency of imidacloprid compared with that of carbaryl was in an agreement with the literature (Table 1). Possible mechanism of the examined insecticides by using GO@TiO_2 under visible light irradiation can be summarized as shown in Scheme 1. The higher photocatalytic properties in the case of GO@TiO_2 compared to GO and TiO_2 may explained by the ability of the surface of graphene oxide to accept electrons from the conduction band (CB) of the metal oxide to react with oxygen generating the superoxide anion radicals ($O_2^{\bullet}-$), which act with the generated reactive $^{\bullet}OH$ radical in decomposing the insecticides molecules into CO_2 and water [49–53].

Table 1
Photo-degradation efficiency of the examined insecticides by the various materials.

Insecticides	Materials	Efficiency	References
Imidacloprid	Photon–Fenton	95%	[44]
	ZnO/$Na_2S_2O_8$	100%	[45]
	TiO_2/$Na_2S_2O_8$	100%	[45]
	Membrane	80%	[46]
	TiO_2	57%	This study
	GO@TiO_2	93%	This study
Carbaryl	Clay	75%	[47]
	Platinum and Boron-doped	90%	[48]
	TiO_2	7%	This study
	GO@TiO_2	22%	This study

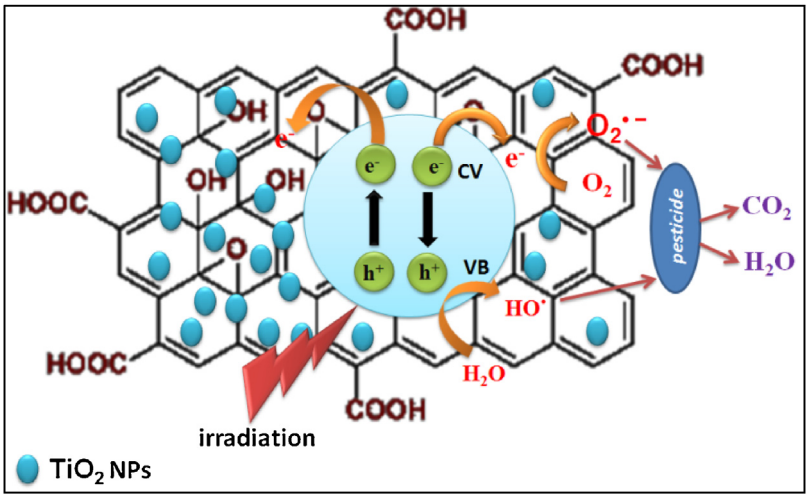

Scheme 1. The proposed mechanism for the photodegradation of the examined insecticides by using GOi@TiO_2.

Adsorption of the examined insecticides on the GO surface

Adsorption of the examined insecticides in the aqueous solution on surface of GO under different concentration levels was examined from the steady-state fluorescence measurements. As shown in Fig. 11, the fluorescence band of the examined insecticides were decreased gradually with increasing the added amounts of GO (0.5 g l^{-1}). The fluorescence quenching may rationalized by the strong binding of the

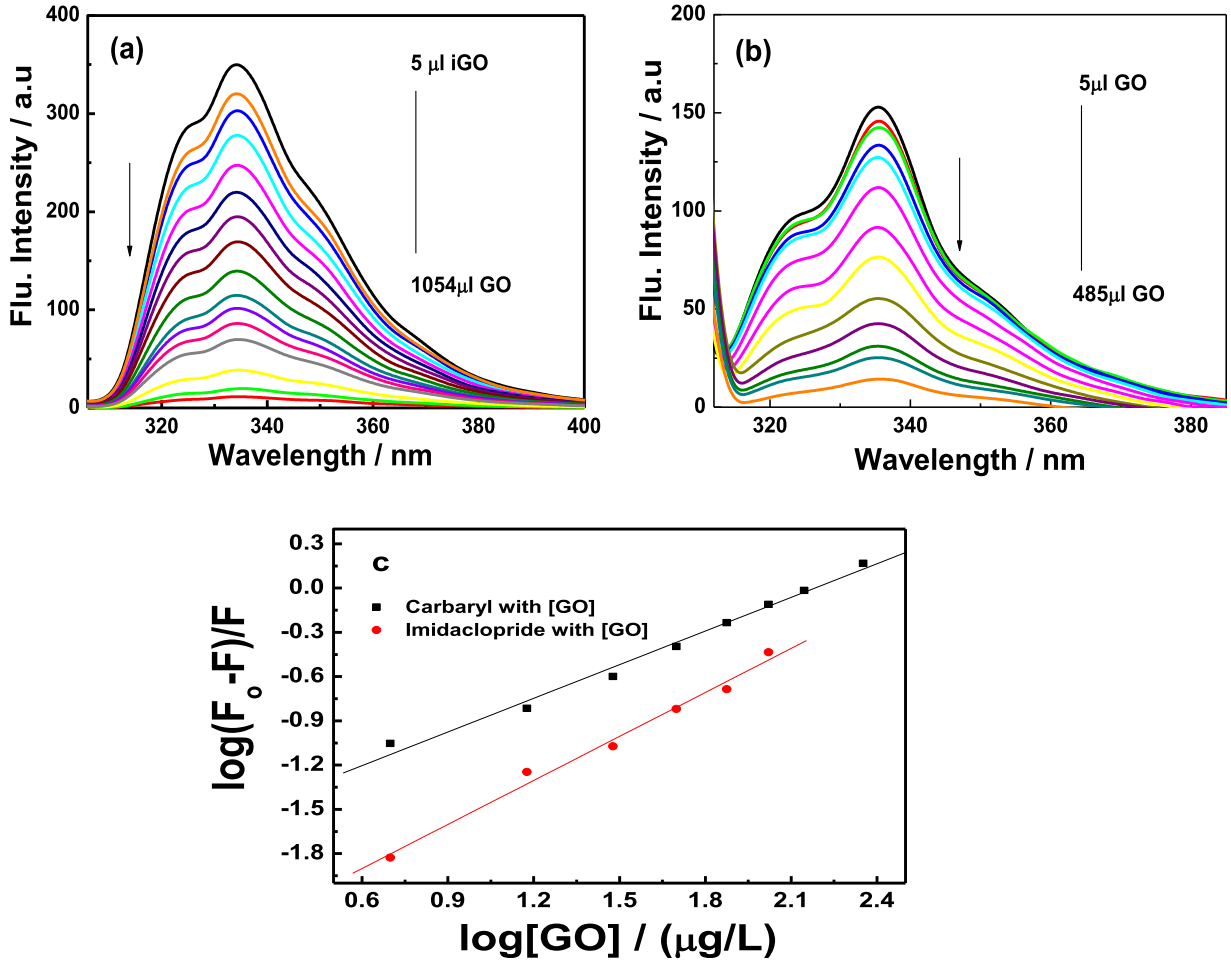

Fig. 11. Fluorescence quenching of: (a) carbaryl, (b) imidocloprid with additions of different amounts of [GO]; λ_{ex} = 300 nm. (c) Linear plot of log (F_0 – F)/F versus log[GO].

examined insecticides with GO through hydrogen bonding, electrostatic interaction and van der waals force [54,55].

Conclusion

TiO_2 NPs and graphene oxide-titanium dioxide (GO@TiO_2) nanocomposite were synthesized and characterized by TEM, XRD UV–vis and SEM. From the optical absorption measurements, the energy band gap values were found to be 4.00, 3.78 and 3.5 eV for GO, TiO_2 and GO@TiO_2, respectively. From the spectroscopic studies, the photocatalytic degradation of examined insecticides by using GO@TiO_2 nanocomposite was found to be more efficient compared to the widely used TiO_2. The highest degradation rate among the examined insecticides was recorded for imidacloprid. Absorption spectroscopy confirmed that the insecticides are efficiently adsorbed over the surface of the graphene oxide. Different features were observed in the presence of metal oxide TiO_2NPs over the surface of graphene oxide such as faster degradation rate of examined insecticides relative to using TiO_2NPs alone. These findings suggest the usefulness the fabricated GO@TiO_2 nanocomposite for degradation the examined toxic insecticides in water.

Conflict of interest

The authors declare no conflict of interest.

Appendix A. Supplementary data

Supplementary data associated with this article can be found, in the online version, at https://doi.org/10.1016/j.jiec.2018.09.045.

References

[1] L. Poirier, B. Lucile, P. Jacquet, C. Lepolard, N. Armstrong, C. Torre, D. Daudé, E. Ghigo, E. Chabrière, Sci. Rep. 7 (2017) 15194.
[2] Q. Wu, X. Zhou, Y. Li, X. Zang, C. Wang, Z. Wang, Anal. Bioanal. Chem. 393 (2009) 1755.
[3] M.G. Vijver, P.J. van den Brink, PLoS One 9 (2013)e89837.
[4] U. EPA, Problem Formulation for Imidacloprid Environmental Fate and Ecological Risk Assessment, US EPA, Washington, DC, 2008 (2011).
[5] W.A. El-Said, M.E. El-Khouly, M.H. Ali, R.T. Rashad, E.A. Elshehy, A.S. Al-Bogami, J. Environ. Chem. Eng. 6 (2018) 2214.
[6] J. Herrmann, C. Duchamp, M. Karkmaz, B.T. Hoai, H. lachheb, E. Puzenat, C. Guillard, J. Hazard. Mater. 146 (2007) 624.
[7] S. Zhang, X. Li, X. Wang, Y. Huang, M. Zeng, J. Xu, J. Mater. Chem. A 3 (2015) 10119.
[8] S. Zhang, Q. Fan, H. Gao, Y. Huang, X. Liu, J. Li, X. Xu, X. Wang, J. Mater. Chem. A 4 (2016) 1414.
[9] S. Zhang, H. Gao, Y. Huang, X. Wang, T. Hayat, J. Li, X. Xu, X. Wang, Environ. Sci. Nano 5 (2018) 1179.
[10] M. Rani, U. Shanker, V. Jassal, J. Environ. Manage. 190 (2017) 208.
[11] S. Sun, X. Zhuang, B. Liu, L. Wang, L. Gu, S. Song, B. Zhang, Y. Chen, Chem. Eur. J. 22 (2016) 2247.
[12] X. Ren, G. Zeng, L. Tang, J. Wang, J. Wan, Y. Liu, J. Yu, H. Yi, S. Ye, R. Deng, Sci. Total Environ. 610–611 (2018) 1154.
[13] X. Ren, G. Zeng, L. Tang, J. Wang, J. Wan, H. Feng, B. Song, C. Huang, X. Tang, Soil Biol. Biotechnol. 118 (2018) 70.
[14] M.R. Gandhi, S. Vasudevan, A. Shibayama, M. Yamada, Chem. Sel. 1 (2016) 4358.
[15] X. Liu, H. Zhang, Y. Ma, X. Wu, L. Meng, Y. Guo, G. Yu, Y. Liu, J. Mater. Chem. A 1 (2013) 1875.
[16] J. Liu, L. Liu, H. Bai, Y. Wang, D.D. Sun, Appl. Catal. B 106 (2011) 76.
[17] N.M. El-Shafai, M.E. El-Khouly, M. El-Kemary, M.S. Ramadan, M.S. Masoud, RSC Adv. 8 (2018) 13323.
[18] W. Sun, A. Du, G. Gao, J. Shen, G. Wu, Microporous Mesoporous Mater. 253 (2017) 71.
[19] V.T. Tran, J.S. Martin, P. Dollfus, S. Volz, Sci. Rep. 7 (2017) 2313.
[20] A. Wei, Y. Li, Y. Li, H. Ye, Comput. Mater. Sci. 138 (2017) 192.
[21] R. Giovannetti, E. Rommozzi, M. Zannotti, C.A. D'Amato, S. Ferraro, M. Cespi, G. Bonacucina, M. Minicucci, A. Di Cicco, RSC Adv. 6 (2016) 93048.
[22] W.S. Hummers Jr., R.E. Offerman, J. Am. Chem. Soc. 80 (1958) 1339.
[23] L.J. Cote, F. Kim, J.X. Huang, J. Am. Chem. Soc. 131 (2009) 1043.
[24] A. Bumajdad, M. Madkour, Y. Abdel-Moneam, M. El-Kemary, J. Mater. Sci. 49 (2014) 1743.
[25] B. Sakthivela, D. Santhakumar, R. Josephineb, K. Sethuramanb, A. Dhakshinamoorthya, Catal. Commun. 108 (2018) 41.
[26] X. Ji, Y. Song, J. Han, L. Ge, X. Zhao, C. Xu, Y. Wang, D. Wu, H. Qiu, J. Colloid Interface Sci. 497 (2017) 317.
[27] M.M. Shahid, P. Rameshkumar, W.J. Basirun, J.J. Ching, N.M. Huang, Electrochim. Acta 237 (2017) 61.
[28] B. Ouadila, O. Cherkaoui, M. Safi, M. Zahouily, Appl. Surf. Sci. 414 (2017) 292.
[29] H. Lia, L. Wang, K. Sheng, L. Zou, B. Ye, Talanta 161 (2016) 838.
[30] H. Shang, D. Han, M. Ma, S. Li, W. Xue, A. Zhang, J. Photochem. Photobiol. B 177 (2017) 112.
[31] S. Woo, Y.-R. Kim, T.D. Chung, Y. Piao, H. Kim, Electrochim. Acta 59 (2012) 509.
[32] M. El-Kemary, N. Nagy, I. El-Mehasseb, Mater. Sci. Semicond. Process. 16 (2013) 1747.
[33] R. Lopez, R. Gomez, J. Sol–Gel Sci. Technol. 61 (2012) 1.
[34] A. Hagfeldt, M. Gratzel, Chem. Rev. 95 (1995) 49.
[35] D. Liang, C. Cui, H. Hu, Y. Wang, S. Xu, B. Ying, P. Li, B. Lu, H. Shen, J. Alloys Compd. 582 (2014) 236.
[36] X. Pan, Y. Zhao, S. Liu, C.L. Korzeniewski, S. Wang, Z. Fan, ACS Appl. Mater. Interfaces 4 (2012) 3944.
[37] H.M. Yadav, J.S. Kim, J. Alloys Compd. 688 (2016) 123.
[38] S.D. Delekar, H.M. Yadav, S.N. Achary, S.S. Meena, S.H. Pawar, Appl. Surf. Sci. 263 (2012) 536.
[39] S.S. Al-Taweel, R.H. Saud, J. Chem. Pharm. Res. 8 (2016) 620.
[40] E. Paek, A.J. Pak, K.E. Kweon, G.S. Hwang, J. Phys. Chem. C 117 (2013) 5610.
[41] M. Sundararajan, L. John Kennedya, P. Nithy, J. Judith Vijaya, M. Bououdin, J. Phys. Chem. Solids 108 (2017) 61.
[42] A. Khataee, S. Arefi-Oskoui, M. Fathinia, A. Fazil, A.S. Hojaghan, Y. Hanifehpour, S.W. Joo, J. Indus. Eng. Chem. 30 (2015) 134.
[43] E. Abdelkader, L. Nadjia, B. Naceur, B. Noureddine, J. Alloys Compounds 679 (2016) 408.
[44] S. Malato, J. Caceres, A. Aguera, M. Mezcua, D. Hernando, J. Vial, A.R. Fernandez-Alba, Environ. Sci. Technol. 35 (2001) 4359.
[45] J. Fenol, I. Garrido, P. Hellin, P. Flores, S. Navarro, Environ. Pollut. Res. 22 (2015) 15055.
[46] Y. Zhang, H. lu, B. Wang, Z. Zhang, X. Lin, Z. Chen, B. Li, Int. Food Sci. Technol. 50 (2015) 1397.
[47] M. Snmez Çelebi, N. Oturan, H. Zazou, M. Hamdani, M.A. Oturan, Sep. Purif. Technol. 156 (2015) 996.
[48] M. El Ouardi, S. Alahiane, S. Qourzal, A. Abaamrane, A. Assabbane, J. Douch, Am. J. Anal. Chem. 4 (2013) 72.
[49] J.A. Khan, M. Qasim, B.R. Singh, S. Singh, M. Shoeb, W. Khan, D. Das, A.H. Naqvi, Spectrochim. Acta A 109 (2013) 313.
[50] B.R. Singh, M. Shoeb, W. Khan, A.H. Naqvi, J. Alloys Compounds 651 (2015) 598.
[51] M. Sundararajana, L.J. Kennedya, P. Nithyab, J.J. Vijayac, M. Bououdinad, J. Phys. Chem. Solids 108 (2017) 61.
[52] S. Huang, Y. Xu, M. Xie, H. Xu, M. He, J. Xia, L. Huang, H. Li, J. Colloids Surf. A 478 (2015) 71.
[53] S. Thennarasu, K. Rajasekar, K.B. Ameen, J. Mol. Struct. 1049 (2013) 446.
[54] E. Abdelkader, L. Nadjia, B. Naceur, B. Noureddine, J. Alloys Compd. 679 (2016) 408.
[55] Y. Yang, S. Song, Z. Zhao, Colloids Surf. A 513 (2017) 315.